Regime Transition in Viscous and Pseudo Viscous Systems: A Comparative Study

Swapna Rabha and Markus Schubert
Inst. of Fluid Dynamics, Experimental Thermal Fluid Dynamics Helmholtz-Zentrum Dresden-Rossendorf, Bautzner Landstraße 400, 01328 Dresden, Germany

Uwe Hampel
Inst. of Fluid Dynamics, Experimental Thermal Fluid Dynamics Helmholtz-Zentrum Dresden-Rossendorf, Bautzner Landstraße 400, 01328 Dresden, Germany

AREVA Endowed Chair of Imaging Techniques in Energy and Process Engineering, Dresden University of Technology, 01062, Dresden, Germany

DOI 10.1002/aic.14528
Published online June 24, 2014 in Wiley Online Library (wileyonlinelibrary.com)

A comprehensive quantitative study on the effect of liquid viscosity ($1 \leq \mu_L \leq 1149$ mPa-s) on the local flow phenomena of the gas phase in a small diameter bubble column is performed using ultrafast electron beam X-ray tomography. The internal dynamic flow structure and the bubble size distribution shows a dual role of the liquid viscosity on the hydrodynamics. Further, the effect of solid concentration ($C_s = 0.05, 0.20$) on the local flow behavior of the gas phase is studied for the pseudo slurry viscosities similar to the liquid viscosities of the gas–liquid systems. The effects of liquid and pseudo slurry viscosities on flow structure, bubble size distribution, and gas phase distribution are compared. The bubble coalescence is significantly enhanced with the addition of particles as compared to the system without particles for apparently same viscosity. The superficial gas velocity at which transition from homogeneous bubbly to slug flow regime occurs is initiated by the addition of particles as compared to the particle free system for apparently same viscosity. © 2014 American Institute of Chemical Engineers *AIChE J*, 60: 3079–3090, 2014
Keywords: liquid viscosity, pseudo slurry viscosity, gas holdup, bubble size distribution, ultrafast electron beam X-ray tomography

Introduction

Slurry bubble column (SBC) reactors have been studied extensively over the past few decades and many articles have already been published on various aspects like fractional gas holdup, axial solid velocity, and bubble size distribution. A review on the existing correlations for the prediction of the gas holdup in SBC reactors can be found in our earlier publications.[1,2] The main influence of the solid concentration in a SBC reactor lies in an increase of the pseudo slurry viscosity of the slurry phase, which suppresses the bubble breakup in the column and attributes to the formation of large and fast moving bubbles, thus, decreases the gas holdup.[3–5] The properties of the liquid–solid suspension can be influenced by size, concentration, and wettability of the particles, as well as by the superficial gas velocity; which in turn increases the shear rate in the liquid and interaction between solid and liquid phase. The suspension behavior of the solid particles in a stationary liquid in terms of the pseudo slurry viscosity was first addressed theoretically by Einstein[6] ($\mu_{sL} / \mu_L = 1 + 2.5\alpha_s$) for small isolated spheres. Since then, various correlations on the pseudo slurry viscosity were developed for a wider range of solid concentrations.[7–11] However, these correlations do not account the effects of particle size, particle shape, particle density, wettability, and superficial gas velocity (Figure 1). In numerical investigations,[12–16] the slurry phase was modeled as a simple single pseudo homogeneous phase, assuming a uniform suspension of the solids in the liquid phase. The assumption of a pseudo homogeneous phase may probably be reasonable for small particles where the particle Reynolds number, Re_P, is below 0.3 and Stokes' law assumption is still valid. However, for larger particles $Re_P > 0.3$, the effect of the solid phase on the liquid cannot be neglected.

Much research has been devoted to the effect of liquid properties on the gas holdup[17–28] over the last decades. The present state of the art of correlations[22–28] predicting the gas holdup in air-water + glycerol systems at $U_G = 0.05$ m/s is summarized in Figure 2. Except for Sotelo et al.,[25] a reduction of the gas holdup with increasing liquid viscosity was observed.[22–28] Apart from the available correlations, there are some controversial reports on the effect of the liquid viscosity on the gas holdup.[19,29–32] An increase of gas holdup was found at low liquid viscosity $\mu \leq 3$–4 mPa-s, a decrease at moderate viscosity $\mu = 3$–11 mPa-s and roughly constant gas holdup at a higher viscosity.[30] With increasing liquid

Correspondence concerning this article should be addressed to S. Rabha at s.rabha@hzdr.de.

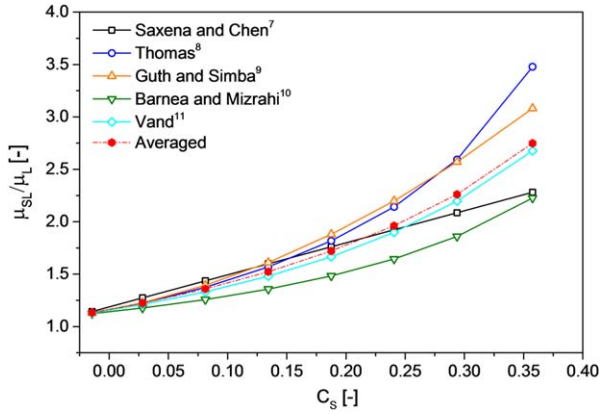

Figure 1. Comparison of the existing correlations for pseudo slurry viscosity as a function of solid concentration.

[Color figure can be viewed in the online issue, which is available at wileyonlinelibrary.com.]

viscosity, the bubble rise velocity reduces due to the large drag force causing an increase in the gas holdup. Conversely, due to the decrease in the rise velocity, the tendency of bubble interactions with each other increases leading to forced coalescence. The increasing coalescence results in large bubbles, which again increases the bubble rise velocity and decreases the gas holdup in the system. Combining these two effects, the liquid viscosity plays a dual role for the gas holdup.[20,32,33] On the contrary, Shollenberger et al.[34] and Chen et al.[35] observed a continuous decrease of the gas holdup with increasing liquid viscosity even at a liquid viscosity of 31 mPa-s.

Similarly, the effect of the addition of solid particles on the gas holdup in a bubble column is in ambiguity. The gas holdup decreases with increasing solid concentration due to the increase of the pseudo slurry viscosity of the slurry phase, which is believed to enhance the bubble coalescence.[3,33,36–40] In our recent articles,[1,2] the "dual effect" of the influence of the particle concentration on the gas holdup at different superficial gas velocities in an SBC was quantitatively studied. An increase in the gas holdup was found for

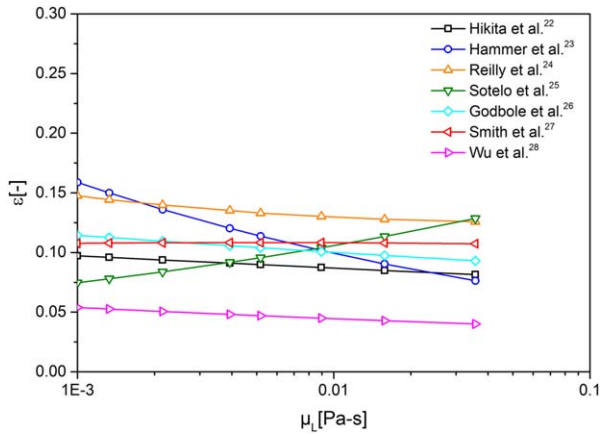

Figure 2. Comparison of the existing correlations for the gas holdup as a function of liquid viscosity (μ_L) for air–water+glycerol systems at $U_G = 0.05$ m/s.

[Color figure can be viewed in the online issue, which is available at wileyonlinelibrary.com.]

Table 1. Viscosities Considered in this Work

Air–Water + Glycerol			Air–Water + Glass Particles			
Glycerol (vol %)	Water (vol %)	Viscosity (μ_L) (mPa-s)	Particle Concentration (wt %)	Viscosity (μ_{sL}) (mPa-s)		
				50 (μm)	100 (μm)	150 (μm)
0	100	1	0	1	1	1
8	92	**1.33**	5	**1.29**	**1.29**	**1.29**
20	80	**2.15**	20	**1.90**	**1.90**	**1.90**
30	70	3.93				
38	62	5.18	–		–	
50	50	8.95	–		–	
60	40	15.8	–		–	
70	30	35.71	–		–	
100	0	1149	–		–	

solid concentration up to 0.03. As solid concentration ($\geq$0.03) further increases, the pseudo slurry viscosity increases and a reduction in the gas holdup was observed. Furthermore, at higher solid concentration ($\geq$0.1), the effect of the solid concentration on the gas holdup was found to be negligible.

The influences of increasing solid concentration in SBCs and of increasing liquid viscosity in bubble columns are qualitatively similar.[3–5] However, the qualitative similarity between the systems was found only based on the average gas holdup, which does not signify the local distribution of the gas phase and the mixing inside the column.[40] No attempt was yet made to compare quantitatively the effect of liquid viscosity in two-phase (gas–liquid) systems and pseudo slurry viscosity in three-phase (gas–liquid–particles) systems on the hydrodynamics under similar operating conditions. Thus, this study is

Figure 3. Snapshot of the in-house developed ultrafast electron beam X-ray tomography along with slug flow at $U_G = 0.034$ m/s and $\mu_L = 1149$ mPa-s (100% glycerol).

[Color figure can be viewed in the online issue, which is available at wileyonlinelibrary.com.]

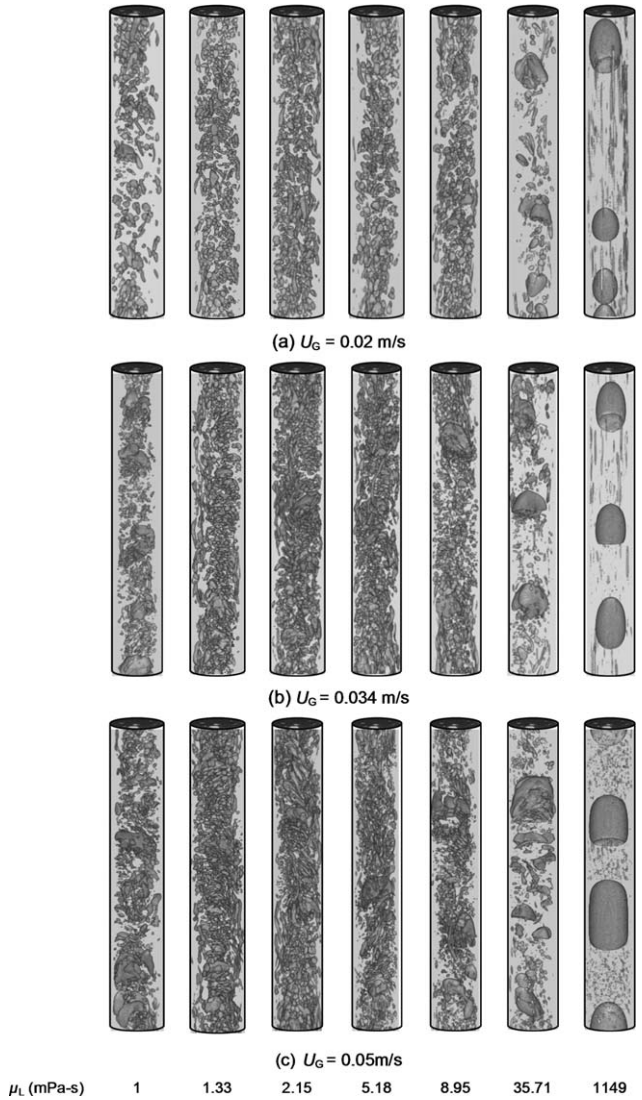

Figure 4. 3-D virtual projection of the gas flow structure at L/D = 8.5 for $1 \leq \mu_L \leq 1149$ mPa-s at U_G = (a) 0.02, (b) 0.034, and (c) 0.05 m/s.

designed to investigate and quantify the effect of liquid viscosity and pseudo slurry viscosity on the local flow phenomena of the gas phase. The radial gas holdup and the approximate bubble size distribution, which describes the gas phase distribution and interfacial area in the bubble columns, were investigated. To look inside particle-laden as well as highly viscous opaque systems at high superficial gas velocity, an "ultrafast electron beam X-ray tomography" imaging technique was used in this work.

Experimental Setup and Ultrafast Electron Beam X-ray Tomography

The experimental setup consists of a cylindrical column of 70 mm inner diameter and 1500 mm height. The gas was distributed through an orifice sparger with 95 holes of 1 mm diameter. The details of the experimental setup are explained by Rabha et al.[1] The pseudo slurry viscosity of the slurry system (water + glass particles) was considered from the average of the predictions calculated from all available correlations[7–11] as shown in Figure 1. The considered diameters of the glass particles were 50, 100, and 150 μm. The viscosities of the liquid mixture (water + glycerol) compositions considered in this work are summarized in Table 1. Two compositions of viscous liquids (water + glycerol) were adjusted to be close to the pseudo slurry viscosities of the slurry phase as indicated in Table 1 (highlighted). The superficial gas velocities considered in this work were 0.02, 0.034, 0.05, 0.07 m/s to cover homogeneous bubbly flow regime and slug flow regime.

The in-house developed ultrafast electron beam X-ray tomography setup[41,42] was used to visualize stacks of cross-sectional images of the flow structure inside the SBC. The details of the experimental tomographic technique and the applied image reconstruction procedure are explained in previous publications.[41,42] A snapshot of the ultrafast electron beam X-ray tomography operating at $\mu_L = 1149$ mPa-s (100% glycerol) and $U_G = 0.034$ m/s is shown in Figure 3. For this experimental work, a temporal resolution of 2000 frames per second for 5 s of measurement was used. The measured scan heights considered in this work were 300, 600, and 950 mm (corresponding to length-to-diameter ratios, L/D = 4.2, 8.5, and 13.57). The reconstructed tomographic data were arranged as a three-dimensional (3-D) voxel with a cross-sectional size of 150 × 150 pixels and a length according to the number of cross-sectional images (10,000 frames). The voxels (image volume elements) of the matrix contain the attenuation of the X-ray due the material distribution in the respective scanning plane. First, the data were binarized by introducing a threshold and the voxels were labeled according to the phase they contain. Voxels

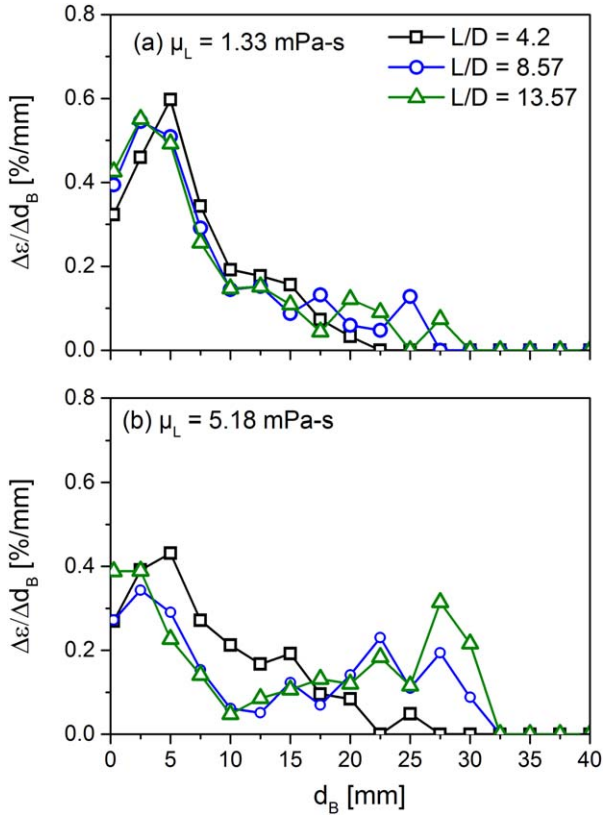

Figure 5. Approximate bubble size distribution at different axial positions L/D = 4.2, 8.57, and 13.57 and U_G = 0.034 m/s for (a) μ_L = 1.33 mPa-s and (b) μ_L = 5.18 mPa-s.

[Color figure can be viewed in the online issue, which is available at wileyonlinelibrary.com.]

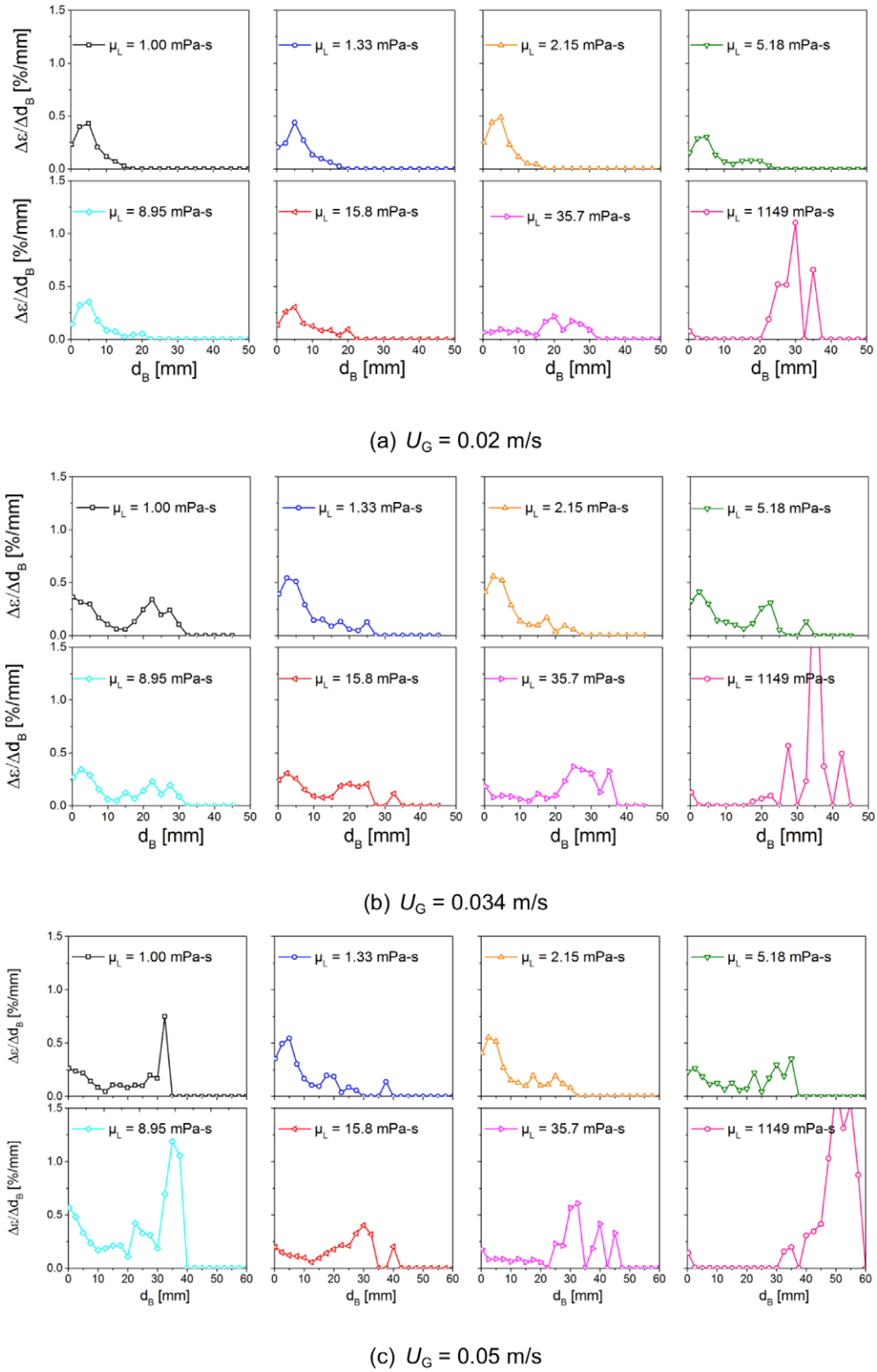

Figure 6. Approximate bubble size distribution for $1 \leq \mu_L \leq 1149$ mPa-s at U_G = (a) 0.02, (b) 0.034, and (c) 0.05 m/s (L/D = 8.5).

[Color figure can be viewed in the online issue, which is available at wileyonlinelibrary.com.]

outside the circular column cross-section were masked out. For this work, a threshold has been selected based on a phantom analysis as 0.47 of the maximum gray value.

The radial gas holdup profile was calculated by averaging the local instantaneous gas fractions over 20 ring-shape domains from the binarized data of 10,000 tomographic images. The approximate bubble size distribution was calculated from 10,000 tomographic images using the algorithm developed by Prasser et al.[43,44] The estimation of bubble size distribution was based on an assumption of constant average

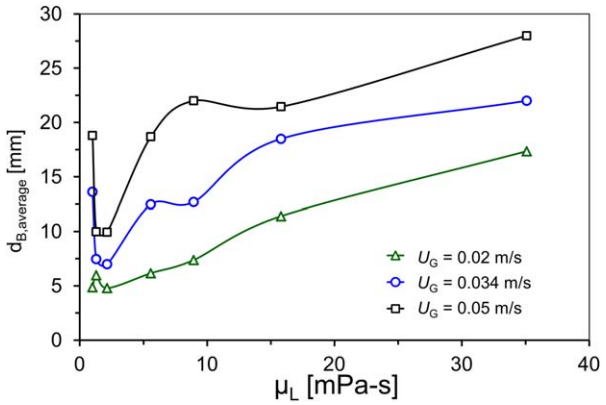

Figure 7. Average bubble diameter as a function of liquid viscosity ($1 \leq \mu_L \leq 15.8$ mPa-s) at $U_G = 0.02$, 0.034, and 0.05 m/s (L/D = 8.5).

[Color figure can be viewed in the online issue, which is available at wileyonlinelibrary.com.]

gas velocity ($w_G = U_G/\varepsilon$). This approximation might not be correct for bubbly flows in large diameter column with pronounced liquid recirculation pattern. However, for smaller column ($D \leq 0.20$ m), where liquid circulation is negligible, this assumption is an appropriate approximation.

Results and Discussion

Effect of liquid viscosity

3-D Virtual Projection of the Gas Flow Structure. The evolving 3-D gas phase flow structures of the gas-liquid two-phase system were visualized from a stack of reconstructed cross-sectional tomographic images. The vertical coordinate of these virtual projections is the time. The virtual 3-D projections of the gas phase flow structure at different liquid viscosities $\mu_L = 1$, 2.15, 5.18, 8.75, 35.71, and 1149 mPa-s for $U_G = 0.02$, 0.034, and 0.05 m/s at L/D = 8.5 are shown in Figures 4a–c, respectively.

At $U_G = 0.02$ m/s, the homogeneous bubbly flow exists until $\mu_L = 8.95$ mPa-s (50% glycerol) as shown in Figure 4a. At higher viscosity, big bubbles were formed due to the bubble coalescence caused by the reduction of bubble rise velocity. At $\mu_L = 1149$ mPa-s (100% glycerol), big bubbles almost equal to the column diameter were observed. At higher gas superficial velocity, with increasing liquid viscosity, less bubbles coalescence was observed as compared to $\mu_L = 1$ mPa-s (air–water) and homogeneous bubbly flow structure was observed up to $\mu_L = 5.18$ mPa-s as shown in Figures 4b,c. Furthermore, at $\mu_L \geq 8.95$ mPa-s (50% glycerol), the population of big bubbles was found to increase due to the reduced bubble rise velocity and finally slug flow at $\mu_L = 1149$ mPa-s (100% glycerol) was observed as shown in Figures 4b,c. The slug flow at $\mu_L = 1149$ mPa-s and $U_G = 0.05$ m/s is photographically confirmed in Figure 3. The bubble slug diameter was found to increase with the superficial gas velocity. The indication of the prevailing flow regime is later explained in the last section of result and discussion. However, the 3-D virtual projections already give a good indication of the prevailing flow regimes.

Approximate Bubble Size Distribution. The approximate bubble size distributions at different axial positions ($4.2 \leq$ L/D ≤ 13.57) for liquid viscosities of $\mu_L = 1.33$ and 5.18 mPa-s at a superficial gas velocity of $U_G = 0.034$ m/s are shown in Figures 5a,b, respectively. The approximate bubble size distributions at different viscosities ($1 \leq \mu_L \leq 1149$ mPa-s) for $U_G = 0.02$, 0.034, 0.05 m/s at L/D = 8.4 are shown in Figures 6a–c, respectively.

The axial position has negligible effect on the bubble size distribution at low liquid viscosity ($\mu_L = 1.33$ mPa-s) as shown in Figure 5a. As the liquid viscosity increases, the effect of the axial position on the bubble size distribution increases and bimodal distribution was observed at higher axial positions indicating bubble coalescence as shown in Figure 5b. However, the difference reduces subsequently at axial position L/D = 8.5. Thus, henceforth in the following sections, all the results are discussed at axial position L/D = 8.5. At $U_G = 0.02$ m/s, with increasing viscosity, the bubble size distribution was narrow and shifts slightly toward smaller bubble diameter up to a viscosity $\mu_L = 8.95$ mPa-s as shown in Figure 6a. With further increase of the viscosity, the bubbles start to coalesce due to the large drag, which reduces the bubble rise velocity. The formation of the big bubbles with diameter of 35 mm was observed at $\mu_L = 1149$ mPa-s (100% glycerol). Similarly, at $U_G = 0.034$ and 0.05 m/s, initially with increasing liquid viscosity, the bubble size distribution becomes narrow up to a liquid viscosity of $\mu_L = 5.18$ mPa-s. At $\mu_L \geq 5.18$ mPa-s, the population of the large bubbles increases, which was indicated by the shift of the bubble size distribution towards large bubble diameters as shown in Figures 6b,c. At pure glycerol ($\mu_L = 1149$ mPa-s), big bubble formation was observed and the diameter of the bubbles increased with superficial gas velocity ($d_B = 40$–45 mm at $U_G = 0.034$ m/s; $d_B = 50$–55 mm at $U_G = 0.05$ m/s). The average bubble diameter was calculated from the bubble size distribution as follows:

$$d_{B,average} = \frac{\sum_{0}^{d_{B,max}} \left(\frac{\Delta\varepsilon}{\Delta d_B}\right) \cdot d_B}{\sum_{0}^{d_{B,max}} \left(\frac{\Delta\varepsilon}{\Delta d_B}\right)} \quad (1)$$

The average bubble diameter as a function of μ_L for $U_G = 0.02$, 0.034, and 0.05 m/s is shown in Figure 7. Initially, a decrease of the average bubble diameter was observed which later starts to increase with increasing viscosity μ_L for all the three velocities. Here, a significant increase of the average bubble diameter with gas superficial velocity was observed.

Gas Holdup. The radial gas holdup profiles which represent the cross-sectional gas phase distribution, are described as a function of the liquid viscosity ($1 \leq \mu_L \leq 15.8$ mPa-s) at $U_G = 0.02$, 0.034, and 0.05 m/s in Figures 8a–c, respectively. The corresponding time-averaged gas holdup calculated at $U_G = 0.02$, 0.034, and 0.05 m/s for $1 \leq \mu_L \leq 15.87$ mPa-s is shown in Figure 9.

At $U_G = 0.02$ m/s, a rather flat radial gas holdup profile was observed for $\mu_L = 1$–15.8 mPa-s. Due to the decrease of the bubble size as reported in the earlier section, an increase of the radial gas holdup profile was observed at lower liquid viscosities of $\mu_L = 1.33$ and 2.15 mPa-s. With further increase of the liquid viscosity, the radial gas holdup profile was found to decrease slightly as compared to the air–water system ($\mu_L = 1$ mPa-s). As U_G increase to 0.034 m/s, the radial gas holdup profile becomes steeper indicating the formation of large bubbles. With the increase of the liquid viscosity, the radial gas holdup profile deviates from that of the air–water system toward lower values. Similar observation was found at $U_G = 0.05$ m/s, however, the

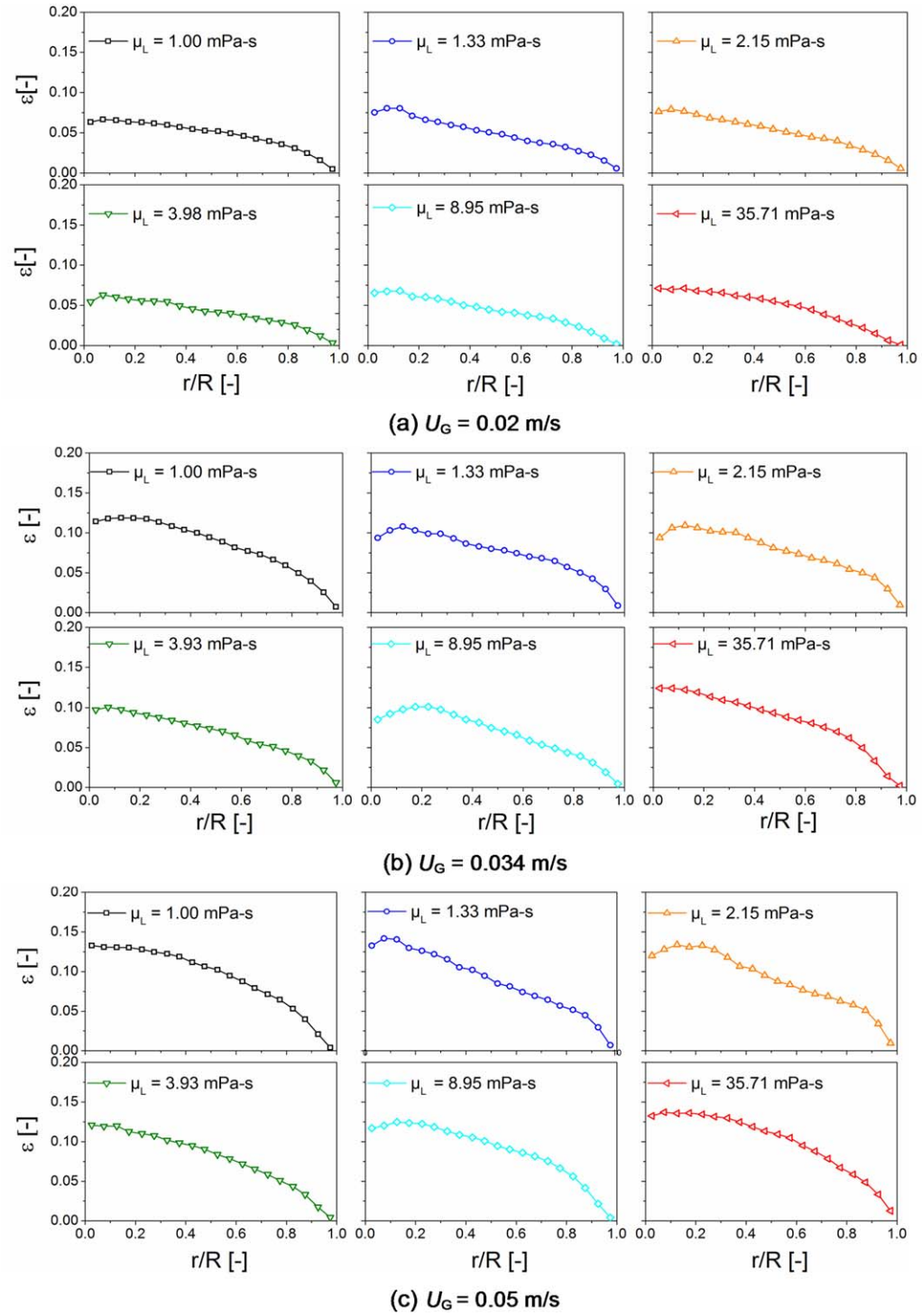

Figure 8. Radial gas holdup profile for $1 \leq \mu_L \leq 15.8$ mPa-s at U_G = (a) 0.02, (b) 0.034, and (c) 0.05 m/s (L/D = 8.5).

[Color figure can be viewed in the online issue, which is available at wileyonlinelibrary.com.]

steepness of the radial profiles increased with an increase of the superficial gas velocity as shown in Figure 8c. Again, an increase in the radial gas holdup profiles at high viscous liquid ($\mu_L = 35.7$ mPa-s) was observed due to the formation of large bubbles at all three gas velocities. Figure 9 shows that the time-averaged cross-sectional gas holdup (ε) increases gradually with the increase of U_G for all μ_L. However, the effect of μ_L on the time-averaged cross-sectional gas holdup was not significant as compared to that of U_G agreeing with the literature.[21,22,24–26]

Comparison of viscous and pseudo viscous systems

3-D Virtual Projection of the Gas Flow Structure. The effects of liquid viscosity ($\mu_L = 1.33$ mPa-s) and pseudo slurry viscosity ($\mu_{sL} = 1.29$ mPa-s) on the gas phase flow

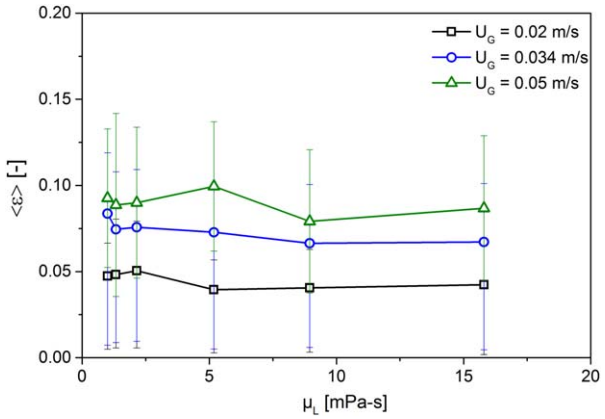

Figure 9. Time-averaged cross-sectional gas holdup as a function of liquid viscosity for $0.02 \leq U_G \leq 0.05$ m/s (L/D = 8.5).

[Color figure can be viewed in the online issue, which is available at wileyonlinelibrary.com.]

structure are visualized at $U_G = 0.02$, 0.034, 0.05 m/s, respectively, in Figures 10a–c. Figure 10 also shows the gas flow structures resulting from the addition of particles with different size ($50 \leq d_P \leq 150$ μm) for same pseudo slurry viscosities ($\mu_{sL} = 1.29$ mPa-s). Figure 11 shows a comparison of the gas flows structure for $\mu_L = 2.15$ and $\mu_{sL} = 1.9$ mPa-s at $U_G = 0.034$ m/s.

From Figures 10 and 11, it is evident that the gas flow structure in the presence of solid particles is significantly different from that without solid particles although the viscosities were almost same. In the presence of particles, the formation of bubbles due to bubble coalescence was observed even at low superficial gas velocity of $U_G = 0.02$ m/s unlike homogeneous bubbly flow in the gas–liquid system for approximately same viscosity. It was also observed that the bubble coalescence increases with increasing superficial gas velocity and particle size as shown in Figure 10.

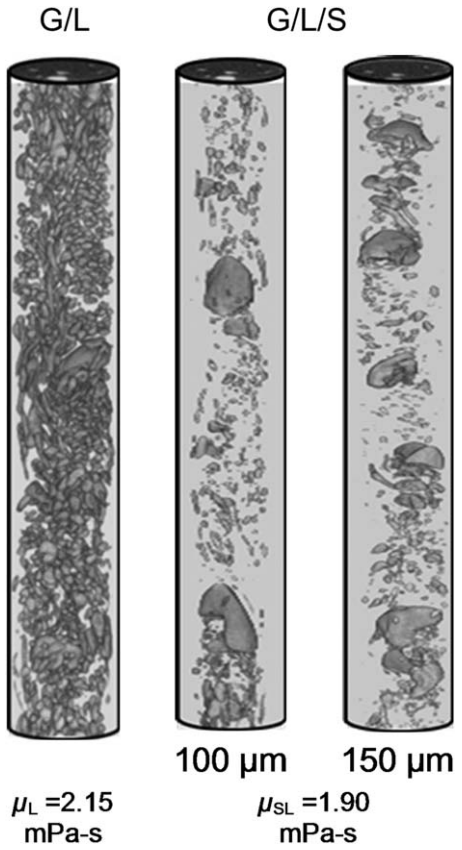

Figure 11. 3-D virtual projection of the gas flow structure for $\mu_L = 1.9$ and $\mu_{sL} = 2.15$ mPa-s at $U_G = 0.034$ m/s and L/D = 8.5.

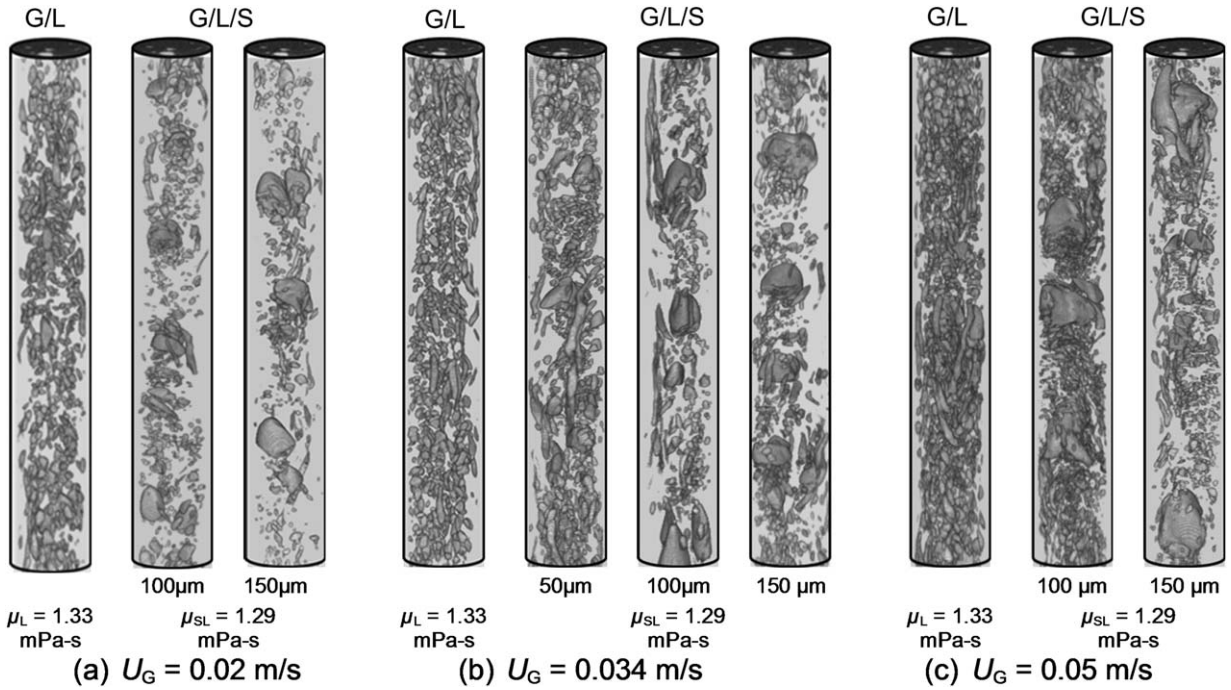

Figure 10. 3-D virtual projection of the gas flow structure for $\mu_L = 1.33$ and $\mu_{sL} = 1.29$ mPa-s at $U_G =$ (a) 0.02, (b) 0.034, and (c) 0.05 m/s (L/D = 8.5).

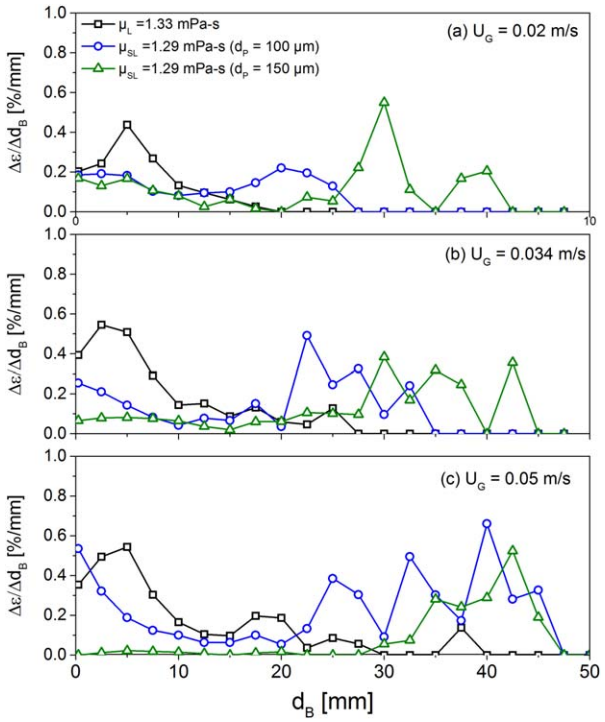

Figure 12. Approximate bubble size distribution for $\mu_L = 1.33$ and $\mu_{sL} = 1.29$ mPa-s at $U_G =$ (a) 0.02, (b) 0.034, and (c) 0.05 m/s (L/D = 8.5).

[Color figure can be viewed in the online issue, which is available at wileyonlinelibrary.com.]

Approximate Bubble Size Distribution. For quantitative comparison between the effects of liquid and pseudo slurry viscosity, approximate bubble size distributions were calculated and compared for $U_G = 0.02$, 0.034, and 0.05 m/s in Figures 12a–c, respectively. For $\mu_L = 1.33$ mPa-s, homogeneous bubble size distribution with a peak local gas holdup at $d_B = 5$ mm was observed at all the three gas superficial velocities $U_G = 0.02$, 0.034, and 0.05 m/s. On the contrary, at $\mu_{sL} = 1.29$ mPa-s with $d_P = 100$ μm, bubble size distributions with peak local gas holdups were observed at $d_B = 22.8$, 22.8, and 40 mm for $U_G = 0.02$, 0.034, and 0.05 m/s, respectively. However, with $d_P = 150$ μm for the same pseudo slurry viscosity $\mu_{sL} = 1.29$ mPa-s, the peak local gas holdups were found at bubble diameter $d_B = 30.3$, 30.3, and 45 mm for $U_G = 0.02$, 0.034, and 0.05 m/s, respectively. The approximate bubble size distributions clearly indicate an enhanced effect of particles on bubble coalescence as compare to particle free systems although the viscosities were almost same.

Gas Holdup. The comparison of the radial gas holdup profiles for $\mu_L = 1.33$ mPa-s and $\mu_{sL} = 1.29$ mPa-s and $\mu_L = 2.15$ mPa-s and $\mu_{sL} = 1.9$ mPa-s at $0.02 \le U_G \le 0.05$ m/s are shown in Figures 13a,b, respectively.

At $U_G = 0.02$ m/s, the difference between the radial gas holdup profiles for both $\mu_L = 1.33$ mPa-s and $\mu_{sL} = 1.29$ mPa-s was not significant. However, with the increase of the superficial gas velocity, the difference between the radial gas holdup profiles for $\mu_L = 1.33$ mPa-s and $\mu_{sL} = 1.29$ mPa-s was increased. The radial gas holdup in the presence of particles ($\mu_{sL} = 1.29$ mPa-s) shows higher values compared to that without particles ($\mu_L = 1.33$ mPa-s). The possible reason

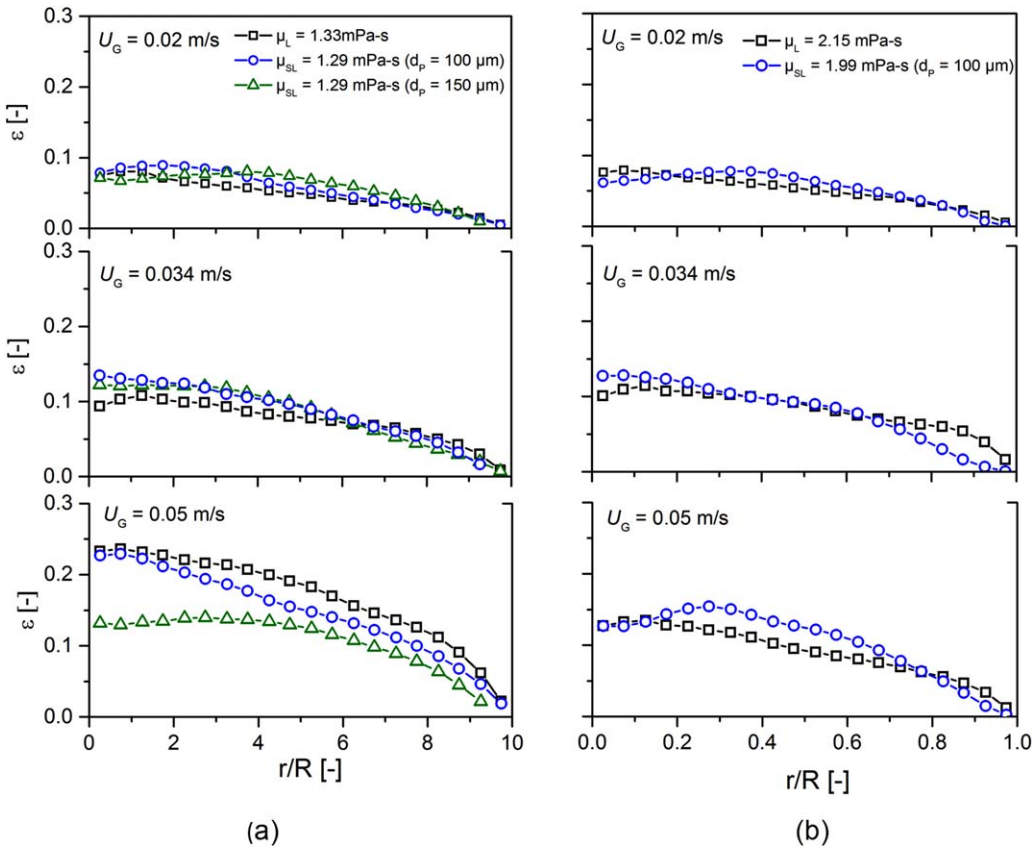

Figure 13. Radial gas holdup profile at $0.02 \le U_G \le 0.05$ m/s for (a) $\mu_L = 1.33$ mPa-s and $\mu_{sL} = 1.29$ mPa-s, (b) $\mu_L = 2.15$ mPa-s and $\mu_{sL} = 1.99$ mPa-s.

[Color figure can be viewed in the online issue, which is available at wileyonlinelibrary.com.]

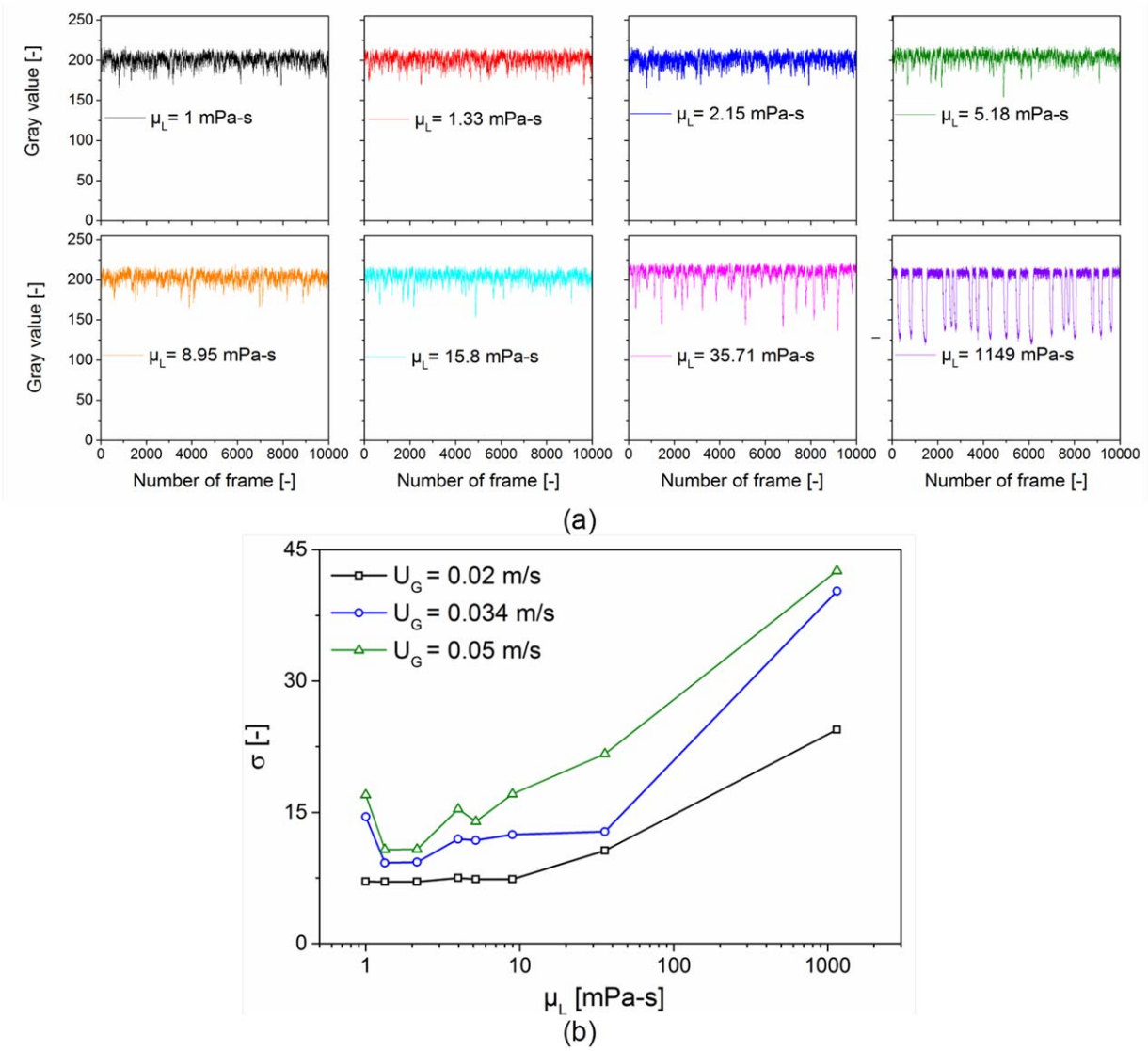

Figure 14. (a) Spatial averaged gray values as a function of time (10,000 images) for $1 \le \mu_L \le 1149$ mPa-s at $U_G = 0.02$ m/s and L/D = 8.5, (b) Standard deviation of the gray value variation over 5 s (10,000 images) for $1 \le \mu_L \le 1149$ mPa-s at $0.02 \le U_G \le 0.05$ m/s and L/D = 8.5.

[Color figure can be viewed in the online issue, which is available at wileyonlinelibrary.com.]

is that the particles promote the bubble coalescence, which causes bubbles to grow until individual bubbles occupy the entire column cross-section indicating slug flow at present experimental condition ($D = 70$ mm).

However, with the increasing liquid and pseudo slurry viscosity ($\mu_L = 2.15$ mPa-s and $\mu_{sL} = 1.9$ mPa-s), the difference between the radial gas holdup profiles without and with solid particles was reduced indicating bubble breakup in pseudo viscous systems with increasing solid concentration as explained in our earlier publications.[1,2]

Flow Regime Comparison. To quantify the prevailing regime more accurately in both viscous (gas–liquid) and pseudo viscous (gas–slurry) systems, further analysis was done for all reconstructed tomographic images based on their gray values without using threshold. Figure 14a shows the spatial averaged gray values at the axial position L/D = 8.5 for 5 s (10,000 images) at $U_G = 0.02$ m/s.

At $\mu_L \le 5.18$ mPa-s, the fluctuations of the gray values were not significant indicating the absence of big bubbles. However, with increasing liquid viscosity ($5.18 \le \mu_L \le 15.81$ mPa-s), few peaks toward the lower gray values were observed which can be correlated with the bubble coalescence and formation of big bubbles. At higher $\mu_L = 35.71$ and 1149 mPa-s, the fluctuations of the gray values significantly increase and large number of peaks were observed toward the lower gray values indicating the presence of big bubbles as shown in Figure 14a.

Furthermore, the standard deviation (σ) of the gray values at the cross-section for gas–liquid flows at liquid viscosities ($1 \le \mu_L \le 1149$ mPa-s) were calculated for $0.02 \le U_G \le 0.05$ m/s and are shown in Figure 14b. At $U_G = 0.02$ m/s, the standard deviation (σ) was almost constant till $\mu_L = 8.51$ mPa-s, indicating that the variation of the gray values was less which can be interpreted as homogeneous bubbly flow regime. The initial sudden decrease of the standard deviation (σ) at $U_G = 0.035$ and 0.05 m/s with increasing the liquid viscosity from 1 to 1.33 mPa-s, confirmed the decrease of bubble size due to the decrease of the surface tension of the liquid. Nonetheless, with further

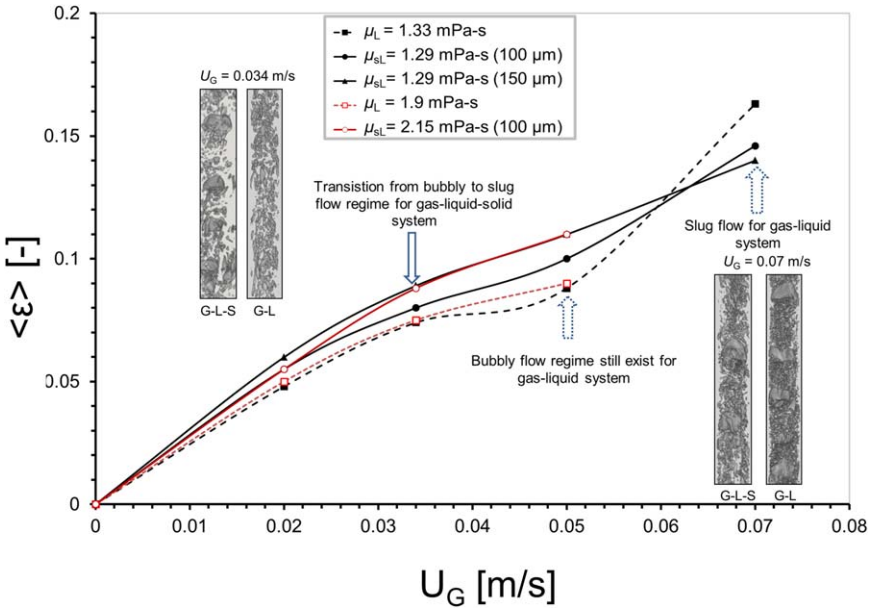

Figure 15. Influence of the superficial gas velocity on the gas holdup and flow regime transition in both viscous and pseudo viscous system.

[Color figure can be viewed in the online issue, which is available at wileyonlinelibrary.com.]

increase of the liquid viscosity, the rise velocity of the bubbles reduces causing the bubble coalescence, which can be shown by the increase of the standard deviation. Finally, at $\mu_L = 35.71$ and 1149 mPa-s, where slug flow was observed in Figure 4 at $0.02 \leq U_G \leq 0.05$ m/s, high values of the standard deviation ($\sigma \sim 17$–43) were observed.

From Figure 14b, it can be concluded that, the critical liquid viscosity at which transition occurs from homogeneous to slug flow regime depends on the superficial gas velocity. At $U_G = 0.02$ m/s, the regime transition was found in the range of liquid viscosity $\mu_L = 8.95$–35.71 mPa-s. Conversely, at higher superficial gas velocities $U_G = 0.034$ and 0.05 m/s, the regime transition was found between liquid viscosity $\mu_L = 3.93$–35.71 mPa-s.

Using the same approach, the transition of the flow regimes from homogeneous bubbly flow to slug flow was also identified approximately for pseudo viscous systems. Figure 15 shows the comparison of the average gas holdup (ε) as a function of the superficial gas velocity for both the viscous and the pseudo viscous system at similar viscosities. The approximated regime transition points along with the snapshots of gas flow structure at $U_G = 0.034$ and 0.07 m/s in both viscous and pseudo viscous systems are embedded in Figure 15.

Similar to the radial gas holdup profile, the average gas holdup in the presence of particles was higher than that without particles at all superficial gas velocities except at $U_G = 0.07$ m/s. At $U_G = 0.07$ m/s, the average gas holdup was high for $\mu_L = 1.33$ mPa-s due to the formation of large bubbles. From Figures 10 and 14, homogeneous bubbly and slug flow regime can be identified at present experimental conditions following the flow regime map of Shah et al.[45] for narrow columns. In the gas–liquid system ($\mu_L = 1.33$ mPa-s), the homogeneous bubbly flow regime exists up to $U_G = 0.05$ m/s, whereupon the transition to the slug flow regimes occurs. Conversely, in the pseudo viscous system ($\mu_{sL} = 1.29$ mPa-s), big bubbles were already observed at low superficial gas velocities ($U_G = 0.02$ m/s) displaying a pronounced slug flow regime with particles at $U_G = 0.034$ m/s as shown in Figures 10 and 11. It can be concluded that the transition point shifted clearly toward lower superficial gas velocity with the addition of particles as compared to systems without particles for the same viscosity.

Conclusions

This work is an attempt to quantify the effect of the liquid viscosity ($1 \leq \mu_L \leq 1149$ mPa-s) on the hydrodynamic flow parameters in gas–liquid system. Furthermore, a comparison has been made between the effects of liquid viscosity ($\mu_L = 1.33$, 2.15 mPa-s) and pseudo slurry viscosity ($\mu_{sL} = 1.29$ and 1.9 mPa-s) on the hydrodynamic parameters at approximately same viscosities and operation conditions. The in-house developed ultrafast electron beam X-ray tomography was used to visualize the dynamic flow structures and to measure the gas holdup and bubble size distributions in both viscous and pseudo viscous systems. From this work, the following conclusions are made.

- The average gas holdup is negligibly affected by liquid viscosity as compared to the pronounced effect of the superficial gas velocity in gas–liquid systems.
- The dual role of the liquid viscosity on the hydrodynamics of gas–liquid flows is proved with the help of bubble size and internal gas flow structure.
- The critical liquid viscosity at which transition occurs from homogeneous to slug flow regime in viscous system depends significantly on the superficial gas velocity.
- Bubble coalescence is significantly enhanced with addition of particles as compared to that without particles at approximately same viscosities and operation conditions.
- An early transition from homogeneous to slug flow regime is initiated in presence of particles as compare to particle free system.

This work shows clearly the difference in the flow behavior of gas–liquid and gas–slurry (liquid + particles) systems

at same liquid and pseudo slurry viscosity, respectively. The outcome of this work clearly shows uncertainties on the application of the two-phase approach (gas phase and slurry phase) based on the pseudo slurry viscosity for the prediction of the hydrodynamics in SBCs, which was applied in many cases in the literature.[8–12]

Notation

C_s = particle concentration
d = diameter, mm
D = column diameter, mm
L = column height at which scan is positioned, mm
Re = Reynolds number
t = time, s
U = superficial velocity, m/s
w = average velocity, m/s

Greek letters

ε = gas holdup
ρ = density, kg m^{-3}
μ = viscosity, mPa-s
σ = standard deviation

subscripts

B = bubble
G = gas
P = particle
L = liquid
SL = pseudo slurry

Literature Cited

1. Rabha S, Schubert M, Wagner M, Lucas D, Hampel, U. Bubble size distribution and gas hold-up distribution in a slurry bubble column using ultrafast electron beam X ray tomography. *AIChE J*. 2013; 59(5):1709–1722.
2. Rabha S, Schubert M, Hampel U. Intrinsic flow behaviour in a slurry bubble column: a study on the effect of particle size. *Chem Eng Sci*. 2013;93:401–411.
3. Vandu CO, Koop K, Krishna R. Large bubble size and rise velocity in bubble column slurry reactor. *Chem Eng Technol*. 2004;27(11): 1195–1199.
4. Zahradnik J, Fialova M, Růžička M, Drahoš J, Kastanek F, Thomas NH. Duality of the gas liquid flow regimes in bubble column reactors. *Chem Eng Sci*. 1997;52:3811–3826.
5. Wang T, Wang J, Jim Y. Slurry reactors for gas to liquid process: a review. *Ind Eng Chem Res*. 2007;46:5824–5847.
6. Einstein A. Eine neue bestimmung der molekuldimensionen. *Ann Phy*. 1906;19:289–306.
7. Saxena SC, Chen, ZD. Hydrodynamics and heat transfer of baffled and unbaffled slurry bubble column. *Rev Chem Eng*. 1994;10:319–400.
8. Thomas DG. Transport characteristics of suspension: VIII. A note on viscosity of newtonian suspensions of uniform spherical particles. *J Colloid Sci*. 1965;20:267–277.
9. Guth E, Simba H. Viscosity of suspensions and solutions: III viscosity of sphere suspensions. *Kolloid-Z*. 1936;74:266–275.
10. Barnea E, Mizrahi JA, Generalized approach to the fluid dynamics of particulate system. Part 1 general correlation for fluidization and sedimentation in solid multi particle systems. *Chem Eng J*. 1973;5: 171–189.
11. Vand V, Viscosity of solutions and suspensions I. Theory. *J Phys Chem*. 1948;52:277–299.
12. Oey R, Mudde R, Portela L, van den Akker H. Simulation of a slurry airlift using a two fluid model. *Chem Eng Sci*. 2001;56:673–681.
13. van Baten J, Ellenberger J, Krishna R. Scale-up strategy for bubble column slurry reactors using CFD simulations. *Catal Today*. 2003; 79–80:259–265.
14. van Baten J, Krishna R. Eulerian simulation strategy for scaling up a bubble column slurry reactor for Fischer-Tropsch synthesis. *Ind Eng Chem Res*. 2004;43:4483–4493.
15. Troshko A, Zdravistc F. CFD modeling of slurry bubble column reactors for Fisher-Tropsch synthesis. *Chem Eng Sci*. 2009;64:892–903.
16. Volker M, Hempel DC. Liquid flow and phase holdup measurement and CFD modeling for two-and three-phase bubble columns. *Chem Eng Sci*. 2002;57:1899–1908.
17. Idogawa K, Ikeda K, Fukuda T, Morooka S. Effect of gas and liquid properties on the behavior of bubbles in a column under high pressure. *Int Chem Eng*. 1987;27:93–99.
18. Zahradnik J, Peter R, Kastanek F. The effect of liquid phase properties on gas holdup in bubble column reactors. *Collect Czech Chem Commun*. 1987;52:335–347.
19. Jamialahmadi M, Müller-Steinhagen H. Effect of alcohol, organic acid and potassium chloride concentration on bubble size, bubble rise velocity and gas holdup in bubble columns. *Chem Eng J*. 1992;50:47–56.
20. Joshi JB, Parasu Veera U, Prasad Ch.V, Phanikumar DV, Deshphande NS, Thakre SS, Thorat BN. Gas holdup structure in bubble column reactors. *PINSA64*. 1998;A(14):441–567.
21. Camarasa E, Vial C, Poncin S, Wild G, Midoux N, Bouillard J. Influence of coalescence behaviour of the liquid and gas sparging on hydrodynamics and bubble characteristic in a bubble column. *Chem Eng Proc*. 1999;38:329–344.
22. Hikita H, Asai S, Tanigawa K, Segawa K, Kitano M. Gas holdup in bubble columns. *Chem Eng J*. 1980;20:59–67.
23. Hammer H, Schrag HJ, Hektor K, Schonau H, Kusters W, Soemarmo A, Sahabi U, Napp W. New sub functions on hydrodynamics, heat and mass transfer for gas/liquid and gas/liquid/solid chemical and biochemical reactors. *Front Chem Reac Eng*. 1984;464.
24. Reilly IG, Scott DS, de Bruijn TJW, Jain A, Piskorz J. A correlation for gas holdup in turbulent coalescing bubble column. *Can J Chem Eng*. 1986;64:705–717.
25. Sotelo JL, Benitez FJ, Beltran-Heredia J, Rodriguez C. Gas holdup and mass transfer coefficient in bubble columns I. Porous glass plate diffusers. *Int Chem Eng*. 1994;34(1):82–90.
26. Godbole SP, Honath MF, Shah YT. Holdup structure in highly viscous Newtonian and non-Newtonian liquids in bubble columns. *Chem Eng Commun*. 1982;16:119–134.
27. Smith DN, Fuchs W, Lynn RJ, Smith DH, Hess M. Bubble behavior in a slurry bubble column reactor model, chemical and catalytic reactor modeling. *ACS Symp Ser*. 1984;237:125–147.
28. Wu Q, Wang X, Wang T, Han M, Sha Z, Wang J. Effect of liquid viscosity on hydrodynamics and bubble behaviour of an external loop airlift reactor. *Can J Chem Eng*. 2013;9999:1–7.
29. Wilkinson PM, Spek AP, van Dierendonck LL. Design parameters estimation for scale-up of high pressure bubble columns. *AIChE J*. 1992;38(4):544–554.
30. Deckwer W. *Bubble Column Reactors*. New York: Wiley, 1991.
31. Eissa SH, Schügerl K. Holdup and backmixing investigations in cocurrent and countercurrent bubble columns. *Chem Eng Sci*. 1975; 30:1251–1256.
32. Ruzicka MC, Drahôs J, Mena PC, Teixeira JA. Effect of viscosity on homogeneous-heterogeneous flow regime transition in bubble column. *Chem Eng J*. 2003;96:15–22.
33. Ong B. Experimental investigation of bubble column hydrodynamics –effect of elevated pressure and superficial gas velocity, Ph.D Dissertation, Washington University, Saint Louis, Missouri, 2003.
34. Shollenberger KA, George DL, Torczynski JR. Effect of liquid viscosity on the development of gas volume fraction profiles in vertical bubble column flows. In: 4th International Conference on Multiphase Flow, New Orleans, LA, May, 2001.
35. Chen J, Gupta P, Degaleesan S, Al-Dahhan MH, Dudukovic MP, Toseland BA. Gas holdup distribution in large diameter bubble columns measured by computed tomography. *Flow Meas Instrum*. 1998;9:91–101.
36. Kara S, Kelkar BG, Shah Y, Carr NL. Hydrodynamics and axial mixing in a three phase bubble column. *Ind Eng Chem Proc Des Dev*. 1982;21:584–594.
37. Krishna R, De Swart JWA, Ellenberger J, Martina GB, Maretto C. Gas holdup in slurry bubble columns: effect of column diameter and slurry concentrations. *AIChE J*. 1997;43(2):311–316.
38. Chilekar VP, Warnier MJF, van der Schaaf J, Kuster BFM, Schouten JC, van Ommen JR. Bubble size estimation in slurry bubble columns from pressure fluctuations. *AIChE J*. 2005;51(7):1924–1937.
39. Behkish A, Lemoine R, Sehabiague L, Oukaci R, Morsi B. Gas holdup and bubble size behaviour in a large-scale slurry bubble column reactor operating with an organic liquid under elevated pressure and temperature. *Chem Eng Sci*. 2007;128:69–84.

40. Shaikh A. Bubble and slurry bubble column reactors: mixing flow regime transition and scale up, Ph.D Dissertation, Washington University, Saint Louis, Missouri, 2007.
41. Fischer F, Hampel U. Ultra-fast electron beam x-ray computed tomography for two-phase flow measurement. *Nucl Eng Des.* 2010; 240(9):2254–2259.
42. Fischer F, Hoppe D, Schleicher E, Mattausch G, Flaske H, Bartel R, Hampel U. An ultra-fast electron beam x-ray tomography scanner. *Meas Sci Technol.* 2008;19:094002.
43. Prasser H-M, Scholz D, Zippe C. Bubble size measurement using wire-mesh sensors. *Flow Meas Instrum.* 2001;12(4):299–312.
44. Prasser H-M, Krepper E, Lucas D. Evolution of the two phase flow in a vertical tube-decomposition of gas fraction profiles according to bubble size class using wire-mesh sensors. *Int J Therm Sci.* 2002;41:17–28.
45. Shah, YT. Gas–Liquid–Solid Reactor Design. New York: McGraw-Hill, 1979.

Manuscript received Mar. 5, 2014, and revision received May 26, 2014.